Polyoxoanion- and Tetrabutylammonium-Stabilized, Near-Monodisperse, 40 ± 6 Å $Rh(0)_{\sim 1500}$ to $Rh(0)_{\sim 3700}$ Nanoclusters: Synthesis, Characterization, and Hydrogenation Catalysis

John D. Aiken III and Richard G. Finke*,†

Colorado State University, Department of Chemistry, Fort Collins, Colorado 80523

Received October 8, 1998

Polyoxoanion- and tetrabutylammonium-stabilized near-monodisperse 40 ± 6 Å $Rh(0)_{\sim 1500}$ to $Rh(0)_{\sim 3700}$ nanoclusters have been prepared by hydrogen reduction, in acetone, of a polyoxoanion-supported Rh(I) complex, $[(n\text{-}C_4H_9)_4N]_5Na_3[(1,5\text{-COD})Rh{\cdot}P_2W_{15}Nb_3O_{62}]$, a reaction in which the resultant Rh(0) nanoclusters serve as a cyclohexene hydrogenation catalyst. The $Rh(0)_{\sim 1500}$ to $Rh(0)_{\sim 3700}$ nanoclusters are isolated as a black powder that can be fully redispersed in non-aqueous solvents such as acetonitrile; they have been characterized by transmission electron microscopy, energy dispersive spectroscopy, electron diffraction, UV−vis spectroscopy, and elemental analysis. Ion-exchange chromatography shows that the isolated Rh(0) nanoclusters are stabilized by the adsorption of the polyoxoanion onto their outer surfaces. Hydrogen gas-uptake stoichiometry, in combination with quantitative kinetic evidence, is presented, indicating that the nanoclusters grow by the slow nucleation, then fast autocatalytic surface-growth, mechanism recently reported for their $Ir(0)_{\sim 300}$ congeners. The *isolated* Rh(0) nanoclusters are also active cyclohexene hydrogenation catalysts in solution; Hg(0) poisoning experiments confirm that the Rh(0) nanoclusters are the active catalyst. These are only the second example of polyoxoanion-stabilized transition-metal nanoclusters; their availability, as well as the record stability and catalytic lifetime in solution of polyoxoanion-stabilized transition-metal nanoclusters, makes possible both fundamental and practical investigations of Rh(0) metal−particle catalysis in solution.

Introduction

Nanoparticle science is an area of explosive recent growth,[1] one in which special interest lies in the synthesis of near-monodisperse (≤±15%)[2] nanoclusters whose size, size-distribution, composition, and shape are controlled via designed synthesis. In 1994 we reported[3,4] the first examples of polyoxoanion- and tetrabutylammonium-stabilized $Ir(0)_{\sim 190-450}$ and $Ir(0)_{\sim 640-1460}$ nanoclusters (abbreviated as $Ir(0)_{\sim 300}$ and $Ir(0)_{\sim 900}$ respectively). These particular transition metal nanoclusters are unusual in the following ways:[2] (i) they contain a novel, highly-charged (9^-) and large-sized (ca. 12 × 15 Å) polyoxoanion nanocluster-stabilizing component, one which provides an unusual *combination* of charge and steric stabilization;[2] (ii) they are among the best com-

† E-mail: rfinke@lamar.colostate.edu.

(1) Reviews on nanoclusters: (a) Jena, P.; Rao B. K.; Khanna, S. N. *Physics and Chemistry of Small Clusters*; Plenum: New York, 1987. (b) Andres, R. P.; Averback, R. S.; Brown, W. L.; Brus, L. E.; Goddard, W. A., III; Kaldor, A.; Louie S. G.; Moscovits, M.; Peercy, P. S.; Riley, S. J.; Siegel, R. W.; Spaepen, F.; Wang, Y. *J. Mater. Res.* **1989**, *4*, 704. This is a Panel Report from the United States Department of Energy, Council on Materials Science on "Research Opportunities on Clusters and Cluster-assembled Materials". (c) Thomas, J. M. *Pure Appl. Chem.* **1988**, *60*, 1517. (d) Henglein, A. *Chem. Rev.* **1989**, *89*, 1861. (e) A superb series of papers, complete with a record of the insightful comments by the experts attending the conference, is available in: *Faraday Discuss., Chem. Soc.* **1991**, *92*, 1−300. (f) Bradley, J. S. In *Clusters and Colloids. From Theory to Applications*; Schmid, G., Ed.; VCH: New York, 1994; pp 459−544. (g) Schmid, G. In *Aspects of Homogeneous Catalysis*; Ugo, R., Ed.; Kluwer: Dordrecht, The Netherlands, 1990; Chapter 1. (h) *Active Metals: Preparation, Characterization, and Applications*; Fürstner, A., Ed.; VCH: Weinheim, Germany, 1996. (i) *Physics and Chemistry of Metal Cluster Compounds*, de Jongh, L. J., Ed.; Kluwer: Dordrecht, The Netherlands, 1994. (j) Schmid, G. *Chem. Rev.* **1992**, *92*, 1709. (k) A Review of Modern Transition-Metal Nanoclusters: Their Synthesis, Characterization, and Applications in Catalysis. Aiken, J. D., III; Finke, R. G. *J. Mol. Catal. A: Chem.* **1999**, in press.

(2) (a) See elsewhere[2b] for a review of nanocluster catalysis which includes necessary key terms and definitions of the following: nanoclusters; traditional colloids; monodisperse and near-monodisperse nanoparticles; "magic number" (i.e., full shell and thus enhanced stability) nanoclusters; Schwartz's updated definition of homogeneous vs. heterogeneous catalysts; inorganic ("charge") and organic ("steric") stabilization mechanisms for colloids and nanoparticles. An overview of the Bu_4N^+ and polyoxoanion-stabilized $Ir(0)_{\sim 300}$ nanoclusters is also provided in that review.[2b] (b) Aiken, J. D., III; Lin, Y.; Finke, R. G. *J. Mol. Cat. A: Chem.* **1996**, *114*, 29−51.

(3) (a) Lin, Y.; Finke, R. G. *J. Am. Chem. Soc.* **1994**, *116*, 8335−8353. (b) Note that in this previous work, it is erroneously reported that an Amberlite IR-400 resin was used for the *cation*-exchange experiment. Amberlite IR-400 resin is, in fact, an *anion*-exchange resin. In the present paper and work, all previously reported cation-exchange experiments were repeated using the appropriate Biorad Amberlite A-27 cation-exchange resin, the same resin used for the cation-exchange experiments reported herein for the Rh(0) nanoclusters.

(4) Lin, Y.; Finke, R. G. *Inorg. Chem.* **1994**, *33*, 4891−4910. This paper reports how we discovered the Ir(0) nanoclusters (by developing a more general solution to the classic "Is it heterogeneous, or homogeneous catalysis" problem). (b) This paper[4] also contains a comparison of the absolute rate of cyclohexene hydrogenation by the Ir(0) nanoclusters to that for an established Ir(0) heterogeneous catalysts. A reviewer inquired whether or not such comparisons are available; in general they are rare, despite their necessity if one is to compare nanocluster catalysts to established catalysts, a point we have made previously.[1k] For this reason, quantitative comparisons of hydrogenation rates of the present Rh(0) nanoclusters, to established Rh heterogenenous and homogeneous catalysts, have been performed and will be reported elsewhere.[13]

10.1021/cm980699w CCC: $18.00 © 1999 American Chemical Society
Published on Web 03/13/1999

positionally characterized transition metal nanoclusters in the literature; (iii) they were designed to be free of catalytic rate-inhibiting surface poisons such as halides, oxides, and hydroxides; and (iv) they are sufficiently stable to be isolated and redissolved in a non-aqueous solution. In addition, (v) they serve as highly active, long-lived "soluble analogs of heterogeneous catalysts", that is, they are active *in solution* without being deposited on a solid support; (vi) they show unprecedented catalytic lifetimes, up to 18 000 total turnovers of cyclohexene hydrogenation in solution; and (vii) their formation can be continuously, and quantitatively, monitored via their reproducible ±15% catalytic hydrogenation activity and the new, "pseudoelementary step kinetic method" we recently reported for following nanocluster nucleation and growth.[5]

Several questions remained, however, despite the above-noted studies of Ir(0) nanoclusters: could we grow other examples of polyoxoanion- and tetrabutylammonium-stabilized nanoclusters, for example Rh(0) (and, later, Pd(0), and Pt(0)) nanoclusters? Would they be formed by the autocatalytic surface-growth mechanism we reported in 1997,[5,6] a mechanism which yields nanocluster size distributions that tend to center around "magic number" full-shell configurations?[7] Would the Rh(0) nanoclusters also be active, long-lived catalysts *in solution* without deposition on a heterogeneous support as is required for most other types of transition-metal nanoclusters?[1k] If so, could we then use the soluble Rh(0) nanoclusters to understand the unique effects that additives like oxygen have on Rh metal particle (heterogeneous) catalysts, notably the increased catalytic activity of both conventional Rh/C and colloidal Rh/C heterogeneous catalysts when exposed to oxygen,[1a] or the effect of O_2 on restructuring or "roughening" of rhodium metal surfaces?[1b] And, what would be revealed by a direct comparison of the second-row Rh(0) and third-row Ir(0) polyoxoanion- and tetrabutylammonium-stabilized nanoclusters? Would the Rh(0) nanoclusters to be more catalytically active as expected but perhaps also less stable due to weaker polyoxoanion-to-nanocluster surface bonding in the case of the second-row Rh(0)?

Herein we report the necessary first step in addressing the questions noted above; specifically we report the following: (i) the synthesis and full characterization of only the second example[8] of polyoxoanion- and tetrabutylammonium-stabilized nanoclusters, near-monodisperse 40 ± 6 Å $Rh(0)_{\sim 1500}$ to $Rh(0)_{\sim 3700}$ nanoclusters.[9] This synthesis is based on our previously developed

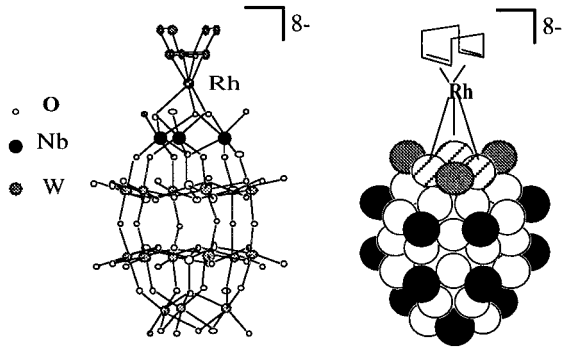

Figure 1. (A) Ball and stick representation and (B) space-filling representation of the (1,5-COD)Rh·$P_2W_{15}Nb_3O_{62}^{8-}$ polyoxoanion-supported nanocluster-forming precatalyst **1**. The Bu_4N^+ and Na^+ counterions have been omitted for clarity. In the space-filling representation the black circles represent terminal oxygens, the white circles represent bridging oxygens, the gray circles represent terminal Nb−O oxygens, and the three hatched circles atop the polyoxoanion to which the Rh is bonded represent the three Nb−O−Nb bridge oxygens. Note that only one of the ≥2 isomers known to be present[10b] for **1** is depicted.

Standard Conditions cyclohexene hydrogenation experiment[3] and begins from the discrete, well-characterized[10] polyoxoanion-supported precatalyst complex, $[(n\text{-}C_4H_9)_4N]_5Na_3[(1,5\text{-COD})Rh\cdot P_2W_{15}Nb_3O_{62}]$, **1**, Figure 1. In addition we report (ii) the characterization of the $Rh(0)_{\sim 1500}$ to $Rh(0)_{\sim 3700}$ nanoclusters by transmission electron microscopy (TEM), energy dispersive spectroscopy (EDS), electron diffraction, UV−visible spectroscopy, elemental analysis, and cation- and anion-exchange chromatography. We also report (iii) kinetic data demonstrating that formation of the Rh(0) nanoclusters proceeds by the slow nucleation and then autocatalytic surface growth mechanism we previously reported,[5] (iv) kinetic data indicating that the Rh(0) nanoclusters are, as expected, faster hydrogenation catalysts than their Ir(0) counterparts, and (v) Hg(0) poisoning experiments demonstrating that the isolated nanoclusters account for all of the observed catalytic activity.

Additional studies of polyoxoanion-stabilized Rh(0) nanoclusters are underway addressing the other issues noted above, specifically their total catalytic lifetime in solution and their O_2-enhanced catalytic activity. Those studies, and the results reported herein, continue our efforts[11] in the synthesis and characterization, mechanism of formation[12] and applications in catalysis[13] of transition-metal nanocluster "soluble analogs of heterogeneous catalysts".[2b]

(5) Watzky, M. A.; Finke, R. G. *J. Am. Chem. Soc.* **1997**, *119*, 10382.
(6) El-Sayed's recent work also provides evidence for a nanocluster surface-growth pathway: Petroski, J. M.; Wang, Z. L.; Green, T. C.; El-Sayed, M. A. *J. Phys. Chem. B* **1998**, *102*, 3316.
(7) Watzky, M. A.; Finke, R. G. *Chem. Mater.* **1997**, *9*, 3083−3095.
(8) We have recently reported a route to 10−40 Å $Rh(0)_n$ nanoclusters by the photolysis of $[(n\text{-}C_4H_9)_4N]_8[Rh(CO)_2\cdot P_2W_{15}Nb_3O_{62}]\cdot(n\text{-}C_4H_9)_4NBF_4$ under H_2. See: Nagata, T.; Pohl, M.; Weiner, H.; Finke R. G. *Inorg. Chem.* **1997**, *36*, 1366.
(9) For other examples of Rh nanoclusters, see: (a) Bönnemann, H.; Brijoux, W.; Brinkmann, R.; Dinjus, E.; Joussen, T.; Korall, B.; *Angew Chem., Int. Ed. Engl.* **1991**, *30*, 1312. (b) Reetz, M. T.; Quaiser, S. A.; *Angew Chem. Int., Ed. Engl.* **1995**, *34*, 2240. (c) Schmid, G. *Struct. Bonding* **1985**, *62*, 51−85. (d) Yonezawa, T.; Tominaga, T.; Richard, D. *J. Chem. Soc., Dalton Trans.* **1996**, 783. (e) Lewis, L. N.; Uriarte, R. J.; Lewis, N. *J. Mol. Catal.* **1991**, *66*, 105−113. (f) See also footnote 8 in: Schmid, G.; Maihack, V.; Lantermann, F.; Peschel, S. *J. Chem. Soc., Dalton Trans.* **1996**, 589−595.

(10) (1,5-COD)M·$P_2W_{15}Nb_3O_{62}^{8-}$ (M = Ir, Rh): (a) Nomiya, K.; Pohl, M.; Mizuno, N.; Lyon, D. K.; Finke, R. G. *Inorg. Synth.* **1997**, *31*, 186−201. (b) Pohl, M.; Lyon, D. K.; Mizuno, N.; Nomiya, K.; Finke, R. G. *Inorg. Chem.* **1995**, *34*, 1413. (c) Pohl, M.; Finke, R. G. *Organometallics* **1993**, *12*, 1453−1457. (d) Finke, R. G.; Lyon, D. K.; Nomiya, K.; Sur, S.; Mizuno, N. *Inorg. Chem.* **1990**, *29*, 1784−1787.
(11) In addition, we recently demonstrated[11a] the use of Cl^-- and $[(C_8H_{17})_3NCH_3]^+$-stabilized Rh(0) nanoclusters as active arene hydrogenation catalysts;[11b] the possibly more interesting, and presumably longer catalytic lifetime, polyoxoanion-stabilized nanoclusters are under investigation.[13] The reader interested in further discussion of the present state-of-the-art in the area of nanoclusters in catalysis, plus some of the outstanding goals for further research, is referred to a recent review.[1k] (a) Weddle, K. S.; Aiken, J. D. III; Finke, R. G. *J. Am. Chem. Soc.* **1998**, 120, 5653−5666. (b) Bönnemann, H.; Brijoux, W. *Active Metals: Preparation, Characterization, Applications*; Fürstner, A., Ed.; VCH: Weinheim, Germany, 1996, p 371. (c) Logan, D. A.; Sharoudi, K.; Datye, A. K. *J. Phys. Chem.* **1991**, *95*, 5568.

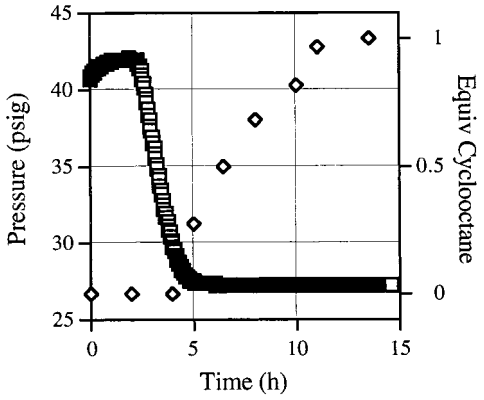

Figure 2. Co-plot of hydrogen pressure (line formed by overlapping squares; left axis) and cyclooctane production by GLC (individual diamonds, right axis) vs time in the hydrogenation of cyclohexene and concomitant formation of near-monodisperse 40 ± 6 Å $Rh(0)_{\sim 2400}$ nanoclusters. A 2.5 ± 0.5 h induction period is seen before the linear H_2 pressure loss, due to cyclohexene hydrogenation, proceeds. The rate, $-d[H_2]/dt$, may be calculated from the slope of the linear portion of the line and is known to be directly proportional[5] to the autocatalytic surface-growth rate constant for the nanoclusters, k_2. [The small rise in pressure sometimes seen as shown in the initial part of Figure 2 varies with solvent (is larger with acetone, but smaller with propylene carbonate) and thus appears to be due to the vapor pressure of the solvent not yet being at equilibrium with the system. A similar rise can occur if the temperature of the Fischer-Porter bottle is initially at a slightly lower temperature than that of the temperature bath.] The individual data for the GLC are as follows: 0.0 equiv, 0 h; 0.0 equiv, 2.0 h; 0.0 equiv, 4.0 h; 0.27 equiv, 5.0 h; 0.50 equiv, 6.5 h; 0.68 equiv, 8.0 h; 0.81 equiv, 10.0 h; 0.96 equiv, 11 h; 1.0 equiv, 13.5 h.

Results and Discussion

Preparation of 40 ± 6 Å $Rh(0)_{\sim 1500}$ to $Rh(0)_{\sim 3700}$ Polyoxoanion- and Tetrabutylammonium-Stabilized Nanoclusters. Near-monodisperse, 40 ± 6 Å Rh(0) nanoclusters were grown *in situ* and isolated by employing our previously developed Standard Conditions hydrogenation reaction (40 psig H_2, 22 °C, 1.65 M cyclohexene) beginning with the polyoxoanion-supported rhodium complex $[(n\text{-}C_4H_9)_4N]_5Na_3[(1,5\text{-COD})Rh{\cdot}P_2W_{15}Nb_3O_{62}]$, **1**, Figure 1. Figure 2 shows the sigmoidal-shaped hydrogen pressure vs time curve (left axis) when beginning with a 1.2 mM solution of **1** in acetone and in the presence of 1.65 M cyclohexene. After a reproducible 2.5 ± 0.5 h induction period during which no hydrogen pressure loss is seen, roughly linear H_2 consumption proceeds at a reproducible rate of $-d[H_2]/dt = 2.4 \pm 0.4$ mmol of H_2/h (when mass transfer limitations are avoided[12]) as cyclohexene is hydrogenated quantitatively to cyclohexane.

The right axis in Figure 2 shows the simultaneous cyclooctane evolution curve from **1** during the nanocluster formation and cyclohexene hydrogenation reaction. This plot reveals that ≤5% of the precursor **1** has been converted into active Rh(0) nanoclusters by the time cyclohexene hydrogenation is complete, a situation somewhat different from that for our analogous Ir(0) nanoclusters (where ca. 45% of the $[(1,5\text{-COD})Ir{\cdot}P_2W_{15}Nb_3O_{62}]^{8-}$ precatalyst evolves into nanoclusters by the time cyclohexene hydrogenation is ca. 85% complete; see Figure 7 elsewhere[3]). The complete hydrogenation of the cyclohexene, by ≤5% of the available Rh, suggests that the $Rh(0)_n$ nanoclusters formed are very active cyclohexene hydrogenation catalysts in solution. Furthermore, the observed high rate of catalytic hydrogenation is consistent with the general trend of increased catalytic activity for second-row vs third-row transition metals. We are pursuing these leads to see just how active and long-lived tetrabutylammonium- and polyoxoanion-stabilized nanoclusters can be; preliminary data has yielded unprecedented nanocluster catalytic lifetimes[1k] in solution, ≤193 000 total turnovers for cyclohexene hydrogenation, results which will be described in detail elsewhere.[13a]

As the nanocluster formation and concomitant cyclohexene hydrogenation reactions proceed, the clear-yellow solution becomes a darker, turbid yellow and eventually deep blue. The blue color, seen previously in the $Ir(0)_{\sim 300}$ and $Ir(0)_{\sim 900}$ nanocluster systems,[3,4] is due to the reversible formation of the $[HP_2W^{VI}{}_{14}W^{V\bullet}Nb_3O_{62}]^{9-}$ heteropolyblue, a one-electron, H•-atom reduced, W(V)• form of the polyoxoanion (an example of "H• spillover",[14] in this case spillover to a novel polyoxoanion soluble oxide.[3]) Once the Rh(0) precatalyst, **1**, has been completely converted into active Rh(0) nanoclusters (after ca. 12 h, as followed by GLC, *vide infra*), the nanoclusters can be isolated as a black powder (by filtration of the reaction solution, or by sedimentation and removal of the reaction solution by pipet, followed by drying under vacuum); the resulting black powder is completely soluble in non-aqueous solvents such as acetonitrile or acetone.

Characterization of the $Rh(0)_{\sim 1500}$ to $Rh(0)_{\sim 3700}$ Nanoclusters by TEM, EDS, Electron Diffraction, UV−Visible Spectroscopy, and Elemental Analysis. Characterization of the isolated Rh(0) nanoclusters was accomplished by TEM, EDS, electron diffraction, UV−visible spectroscopy, and elemental analysis. TEM images of a clear amber acetonitrile solution of isolated Rh(0) nanoclusters redispersed onto a TEM grid, Figure 3, show nonaggregated, near-monodisperse (i.e. ≤±15% dispersion[2b]) 40 ± 6 Å Rh(0) nanoclusters.[15] EDS analysis detects Rh, O, Nb, and W, confirming that both rhodium and the polyoxoanion, $P_2W_{15}Nb_3O_{62}^{9-}$, are present[16] (Supporting Information, Figure A). Electron diffraction indicates that the metal core of the nanoclusters consists of ccp Rh(0) metal, as determined by matching the 220, 311, and 420 *d*-spacings of the Rh(0)

(12) We have recently used Rh(0) nanoclusters to demonstrate the effect that H_2 gas-to-solution mass-transfer limitations have on the resulting nanoclusters, namely the need to avoid mass-transfer conditions in the synthesis of near-monodisperse nanoclusters: Aiken, J. D., III; Finke, R. G. *J. Am. Chem. Soc.* **1998**, *120*, 9545−9554.

(13) (a) Aiken, J. D., III; Finke, R. G. Polyoxoanion- and Tetrabutylammonium-Stabilized $Rh(0)_n$ Nanoclusters: Unprecedented Nanocluster Catalytic Lifetime In Solution, in preparation. (b) Aiken, J. D., III; Finke, R. G. A Comparison of CS_2 Catalyst Poisoning of 5% Rh/Al_2O_3 To Polyoxoanion- and Tetrabutylammonium-Stabilized Rh(0) Nanoclusters, in preparation.

(14) Pope, M. T. *Heteropoly Blues in Mixed Valence Compounds*; Brown, D. B., Ed., Reidel: Dordrecht, The Netherlands, 1980; p 365.

(15) Interestingly, the 20 and 40 Å diameters of our iridium and rhodium nanoclusters, respectively, are close to those seen for Ir and Rh nanocolloids synthesized elsewhere using alcohol reductants, Os (~ < 10 Å) < **Ir (14−30 Å)** < Pt (27 Å) < **Rh (~40 Å)** < Pd (53 Å). See Hirai, H.; Nako, Y.; Toshima, N.; *J. Macromol. Sci.−Chem.* **1979**, *A13* (6), 727. Also, 38 ± 7 Å Rh nanoclusters are reported when $[Rh(H_2O)_6]^{3+}$ is reduced under H_2 in the presence of trisodium citrate in water.[9f]

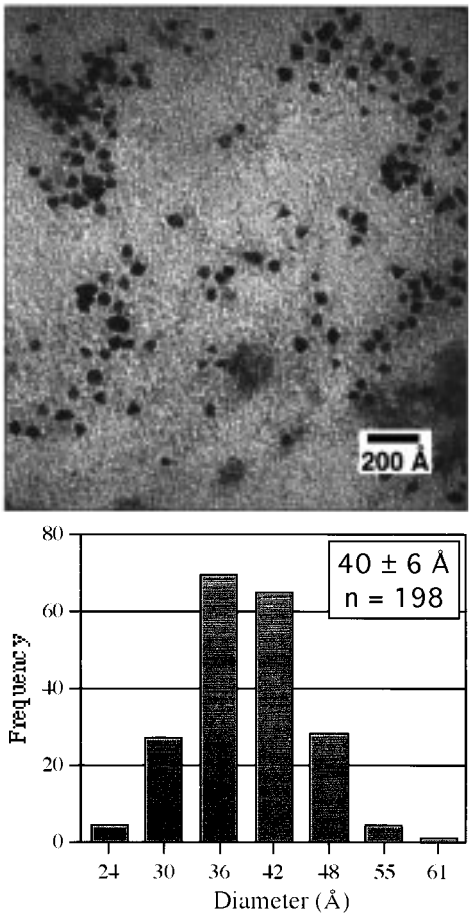

Figure 3. TEM image (250K magnification) and associated particle size histogram ($n = 198$ particles counted) of isolated, near-monodisperse 40 ± 6 Å (4.0 ± 0.6 nm) $Rh(0)_{\sim 2400}$ nanoclusters grown by the reduction of 1.2 mM **1** in acetone under the standard conditions described in the Experimental Section which include 22 °C and 40 ± 1 psig H_2. The sample was harvested after 100% conversion of **1** into nanoclusters as determined by the complete release of the expected 1.0 equivalent of cyclooctane produced from **1** (100% by GLC analysis).

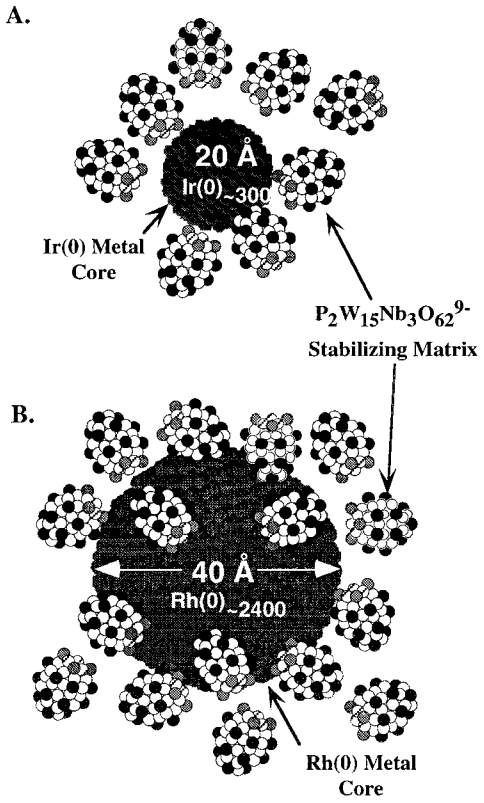

Figure 4. Roughly-to-scale images of *idealized* metal cores of a perfect 20 Å $Ir(0)_{\sim 300}$ nanocluster (A, top) and a perfect 40 Å $Rh(0)_{\sim 2400}$ nanocluster (B, bottom). The models were created using Biograf 3.21 from the known lattice constants of fcc bulk Ir and Rh metals, 3.84 and 3.80 Å respectively. In the 20 Å Ir(0) nanocluster, ~50% of the metal atoms are on the surface, whereas, in the 40 Å Rh(0) nanocluster, ~30% of the metal atoms are on the surface. For the sake of clarity, only a portion of the polyoxoanions known to be present is shown, the polyoxoanion is shown in its monomeric, $P_2W_{15}Nb_3O_{62}^{9-}$ form (and not in its Nb−O−Nb bridged anhydride form[3]), and the Bu_4N^+ and Na^+ cations have been deliberately omitted.

nanoclusters to literature values[17] for authentic Rh(0) ccp metal (Supporting Information, Figure B). A UV−visible spectrum of the nanoclusters in acetonitrile (Supporting Information, Figure C) shows no maximum, only an increasing shoulder from the visible into the UV, as predicted for rhodium particles in the nanometer size regime.[18]

The diameter of the Rh(0) nanoclusters (40 ± 6 Å) is approximately twice as large by TEM as the diameter of Ir(0) nanoclusters (20 ± 3 Å) isolated under identical conditions. This mirrors the decrease in metal particle size seen for Rh vs Ir nanoclusters in the literature where, for example, polymer-stabilized colloidal dispersions of Rh and Ir prepared in methanol−water solutions are 40 and 14 Å, respectively.[15] An idealized image of a 40 Å $Rh(0)_{\sim 2400}$ nanocluster, along with a portion of its stabilizing polyoxoanion component, is shown in Figure 4 (bottom, part B). Also shown for comparison is our previously isolated 20 Å $Ir(0)_{\sim 300}$ (Figure 4, top, part A). Noteworthy is that while the 20 Å $Ir(0)_{\sim 300}$ nanocluster has ca. 50% of its metal atoms on the surface, the 40 Å $Rh(0)_{\sim 2400}$ nanocluster has only ca. 30% of its metal atoms on its surface. The observed, near-monodispersed 40 ± 6 Å size range of the Rh(0) nanoclusters corresponds to the limits of 34 Å $Rh(0)_{\sim 1500}$ to 46 Å $Rh(0)_{\sim 3700}$.[19] As before,[3] we *represent* the *average* 40 Å clusters by the *convenient approximation* $Rh(0)_{\sim 2400}$, but emphasize that such a designation *approximates only the average size.* In addition, although

(16) As expected, peaks for Na, Cr, and Cu are also seen in the EDS spectrum. Na is present as a countercation (from the precursor **1**) whereas the Cr peak comes from the specimen holder and the Cu peak comes from the copper grid. Peaks for C and N are not seen since they are below the limit of detection.

(17) The literature values for Rh(0) and Au(0) *d*-spacings were obtained from: PDF-2 Database Sets 1-42, Powder Diffraction File, International Centre for Diffraction Data, 1992.

(18) The plasmon resonance gives rise to this tailing absorption; for a compilation of the absorption spectra of several colloidal metallic elements, see: Creighton, J. A.; Eadon, D. G.; *J. Chem. Soc., Faraday Trans.* **1991**, *87*, 3881.

(19) The 40 ± 6 Å, or 34 to 46 Å, $Rh_{\sim 1500}$ to $Rh_{\sim 3700}$ approximate metal content numbers were calculated using the equation $N = N_o rV/MW$ where $N_o = 6.02 \times 10^{23}$ atoms/mol, $r = 12.41$ g/cm^3, $V = 4/3\pi(D/2)^3$, and MW = 102.9. This equation shows that a spherical 40 Å rhodium particle contains ≈ 2430 metal atoms, whereas 34 and 46 Å rhodium particles contain ≈ 1500 and 3700 metal atoms, respectively. While the values of 1500 and 3700 metal atom particles are close to the number of atoms predicted in so-called "magic number" clusters (at 1415 and 3871), the number of atoms in a 40 Å rhodium particle (≈2430) falls in between the two magic numbers values of 2057 and 2869.

our previous 20 ± 3 Å $Ir(0)_{\sim 300}$, and the related 30 ± 4 Å $Ir(0)_{\sim 900}$, nanoclusters both center about the magic numbers $Ir(0)_{309}$ and $Ir(0)_{923}$, a perfectly spherical 40 Å Rh particle would contain ca. 2430 metal atoms[19] and thus would fall *in between* the two idealized magic number values of 2057 and 2869. Such deviations from magic numbers are predicted as metal particle size increases, since the difference in energy between each magic-number-sized, full-shell nanocluster becomes smaller as the nanoclusters themselves become larger.[20,21]

Interestingly, a closer examination of the TEM image in Figure 3 reveals that 8% (i.e., ca. 30 out of 380) of the individual Rh(0) nanoclusters appear to have a triangular, rather than roughly spherical, shape. One possibility for this shape difference is that the electron beam of the TEM is causing metal core rearrangement—a well-documented phenomena with various ligand-stabilized metal particles in this size regime.[1k,22] A second possibility is that tetrahedral nanoclusters are formed directly in the reaction, a possibility that has literature precedent,[23] including in a Pt nanocluster system which has also been reported to grow by a surface-growth mechanism[6] (the distribution of differently shaped Pt nanoparticles grown under H_2 varies with changes in capping polymer, the Pt^{2+} concentration, and the pH and includes particles with tetrahedral, cubic, irregular-prismatic, icoshedral, and cubo-octahedral shapes[6,24]). The different nanocluster shapes are attributed to differences in the growth rates on the Pt nanocluster's {111} and {100} crystalline faces.[6] El-Sayed further reports that capping of the {111} face of the Pt nanoparticles by the stabilizing polyacrylate polymer forces surface growth on the {100} face, resulting in tetrahedral particles.[6] As both Pt and Rh are cubic close packed metals, at least in the bulk state,[25] it is possible that a similar process could be occurring in our present $Rh(0)_{\sim 2400}$ system as well.

Elemental analysis was obtained on four samples of isolated $Rh(0)_{\sim 2400}$ nanoclusters and then averaged to determine the approximate ratio of Rh metal atoms to the $P_2W_{15}Nb_3O_{62}^{9-}$ polyoxoanion. The composition of the $Rh(0)_{\sim 2400}$ nanoclusters which is best fit by the elemental analysis data (average of four samples, including a repeat analysis on two) is $[Rh_{\sim 7}(P_4W_{30}Nb_6O_{123})TBA_{\sim 5.5}Na_{\sim 10.5}]_{\sim 340}$, a formulation which indicates that there are approximately seven Rh metal atoms for every polyoxoanion (in its anhydride, Nb−O−Nb bridged $P_4W_{30}Nb_6O_{123}$ form; see ref 3).[26]

Hydrogen Gas-Uptake Stoichiometry During the Formation of Rh(0) Nanoclusters and Its Comparison to Ir(0). A hydrogen gas-uptake experiment was performed in order to verify the reaction stoichiometry during the formation of Rh(0) nanoclusters from **1**. Under a H_2 pressure of 273 Torr, and after an induction period of ca. 4 hrs, 9 mM **1** (in propylene carbonate, and at 22.7 °C) consumes 3.9 ± 0.4 equiv hydrogen per mole Rh, Figure 5, and releases 1.0 ± 0.1 equiv of cyclooctane (by GLC). During this experiment, the original dark-amber orange solution changed to brown, then to dark brown/black, and eventually to dark blue/black as the heteropolyblue form of the $P_2W_{15}Nb_3O_{62}^{9-}$ polyoxoanion is formed. (A control experiment confirmed that the Rh(0) nanoclusters formed in this particular experiment are also active catalysts, hydrogenating cyclohexene with no detectable induction period.)

This reaction stoichiometry can be rationalized, as before for our polyoxoanion-stabilized Ir(0) nanoclusters,[3,27a] by Scheme 1, in which 2.5 equiv of H_2 are used to produce one equivalent each of cyclooctane and Rh(0) from the $[(1,5\text{-COD})Rh(I)]^+$ moiety (step I); then, an additional 1.0 equiv of H_2 is required to produce the 2 e^- reduced, 2 e^- heteropolyblue form of the polyoxoanion (step IV). This scheme, and the resultant stoichi-

(20) Schmid correctly notes that "The higher the number the metal atoms the more probable deviations from the ideal magic number will be. The controlled synthesis of such large, chemically stabilized clusters will become more difficult going from shell to shell." Developments in Transition Metal Cluster Chemistry—The Way to Large Clusters. Schmid, G. *Struct. Bonding* **1985**, *62*, 51.

(21) (a) Indeed, some nanoclusters, such as those of Si_x or Na_x, are believed to have "fluidlike" surfaces, with many structures within even 0.1 eV above the equilibrium structures. See Brus and Siegel's discussion, especially p 719 in the reference which follows, where they note that "total energy calculations have shown that there are many metastable configurations in a 0.1 eV (i.e., 2−3 kcal/mol) range above the equilibrium state, and that their number increases significantly with the cluster size": Research Opportunities on Clusters and Cluster-Assembled Materials—A Department of Energy, Council on Materials Science Panal Report. Andres, R. P.; et al. *J. Mater. Res.* **1989**, *4*, 704; see p 719. (b) Martins, J. L.; Buttet, J.; Car, R. *Phys. Rev. B* **1985**, *31*, 1804. (c) Ballone, P.; Andreoni, W.; Car, R; Parrinello, M. *Phys. Rev. Lett.* **1988**, *60*, 271.

(22) (a) For the aggregation of Au clusters under the TEM electron beam see: Schmid, G. *Struct. Bonding* **1985**, *62*, 51−85. (b) For an account where the stabilizing ligand shell is lost and the Au nuclei rearrange see: Schmid, G. *Polyhedron* **1988**, *7*, 2321−2329. (c) For the observation of rapid changes in the structure and size of Pt_{55} clusters, and for accounts of mobile surface atoms in nanoclusters under a TEM beam, see: Schmid, G. *Chem. Rev.* **1992**, *92*, 1709−1727. (d) For individual crystallite aggregation under a TEM beam see: Che, M; Bennet, C. O. *Adv. Catal.* **1989**, *36*, 55. (e) For loss of ligands, and reduction and relaxation of the metal core, of Pd particles under a TEM beam, see: Volkov, V. V.; Van Tendeloo, G.; Tsirkov, G. A.; Cherkashina, N. V.; Vargaftik, M. N.; Moiseev, I. I.; Novotortsev, V. M.; Kvit, A. V. and Chuvilin, A. L. *J. Cryst. Growth* **1996**, *163*, 377. (f) See also ref 18 in ref 3.

(23) Duff, D. G.; Curtis, A. C.; Edwards, P. P.; Jefferson, D. A.; Johnson, B. F. G.; Logan, D. E. *J. Chem. Soc., Chem. Comm.* **1987**, 1264−1266.

(24) (a) Ahmadi, T. S.; Wang, Z. L.; Green, T. C.; Henglein, A.; El-Sayed, M. A. *Science* **1996**, *272*, 1924−1926. (b) Ahmadi, T. S.; Wang, Z. L.; Henglein, A.; El-Sayed, M. A. *Chem. Mater.* **1996**, *8*, 1161−1163. (c) Additionally, the structure of Pt nanoclusters in a second system can be converted from icosahedral to cuboctahedral by changing the stabilizing ligand from CO to PPh_3. See: Rodriguez, A.; Amiens, C.; Chaudret, B.; Casanove, M.-J.; Lecante, P.; Bradley, J. S. *Chem. Mater.* **1996**, *8*, 1978.

(25) See Table 29.3 in: Wells, A. F. *Structural Inorganic Chemistry*, 4th ed.; Clarendon Press: Oxford, England, 1975; p 1015.

(26) It is important to note that the isolation procedure used herein to isolate the Rh(0) nanoclusters is not optimum for elemental analysis in that we decant away the reaction solution, a procedure which leaves excess polyoxoanion behind. (We are currently developing improved nanocluster isolation procedures on larger synthetic scales.[26b]) As a result, given that the nanoclusters are not one discrete, exact molecule but a distribution of particles, we found some scatter in the C and N values among the four batches, scatter that is presumably due to a sampling error in the somewhat inhomogeneous sample (Table A, Supporting Information), a phenomenon which has been observed by others for isolated Pd nanoclusters.[26c] However, given the *at least* ±0.84% error and ±0.51% error for C and N in the analytical data itself (determined by repeat analyses on identical samples, Table A, Supporting Information), all analyses of the $Rh(0)_{\sim 2400}$ nanoclusters are within experimental error of the stated empirical formula. (b) Polyoxoanion- and Tetrabutylammonium-Stabilized Transition Metal "Soluble Analogs of Heterogeneous Catalysts": Scaled Up Synthesis and the Effect of Solvent on the Isolability and Catalytic Activity of Ir(0) Nanoclusters. Aiken, J. D., III; Müller, F.; Finke, R. G. Manuscript in preparation. (c) Note that others have reported that, in three ostensibly identical preparations of Pd nanoclusters in DMSO, elemental analyses of the isolated Pd nanoclusters varied as much as 5.61% for C, 1.01% for H, and 2.02% for S. See: van Bentham, R. A. T. M. *Palladium Cluster Catalyzed Oxidative Cyclizations in the Synthesis of Aminoalkenols and Diamines*; University of Amsterdam: Amsterdam, 1995; Chapter 8, p 130.

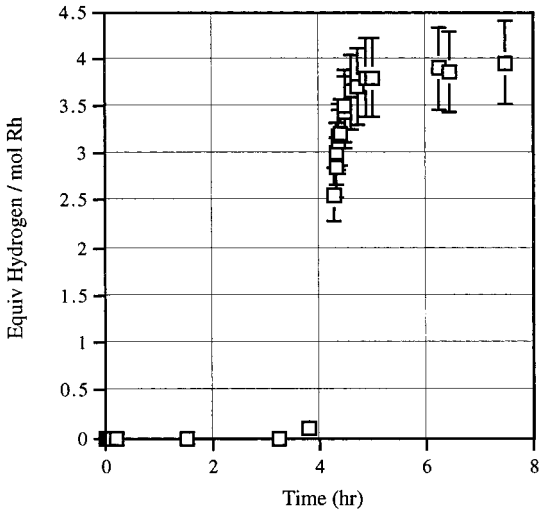

Figure 5. Plot showing the smooth, sigmoidal (autocatalytic[5]) uptake of 3.9 ± 0.4 equiv of H_2/mol of **1**.

Scheme 1. Equations Which Rationalize the Uptake of 3.5 equiv of H_2 per Mole of 1 during the Formation of the Rh(0) Nanoclusters[a]

$$(1,5\text{-COD})Rh{\bullet}P_2W_{15}Nb_3O_{62}^{8-} + 2.5\ H_2 \longrightarrow \quad \text{(I)}$$

$$\text{(cyclooctane)} + Rh(0) + H^+ + P_2W_{15}Nb_3O_{62}^{9-}$$

$$n\ Rh(0) \longrightarrow Rh(0)_n \quad \text{(II)}$$

$$P_2W_{15}Nb_3O_{62}^{9-} + H^+ \longrightarrow 0.5\ P_4W_{30}Nb_6O_{123}^{16-} + 0.5\ H_2O \quad \text{(III)}$$

$$0.5\ P_4W_{30}Nb_6O_{123}^{16-} + H_2 \longrightarrow 0.5\ P_4W^{VI}{}_{26}W^{V}{}_4Nb_6O_{123}^{20-} + 2\ H^+ \quad \text{(IV)}$$

[a] This scheme summarizes the production of 1 equiv of cyclooctane, the formation of Rh(0) metal atoms from the Rh(I) complex, and the formation of the reduced, W(V)-containing heteropolyblue form of the polyoxoanion.

ometry of 3.5 equiv of H_2 per **1**, are consistent with the experimental observables of (i) the formation of 1 equiv of cyclooctane from the precatalyst **1** (by GLC), (ii) the reduction of the Rh(I) complex to Rh(0) metal (by electron diffraction), and (iii) the formation of a two-electron reduced heteropolyblue (i.e., as determined previously[3]) via hydrogen spillover to the polyoxoanion.

Although the number of hydrogen equivalents consumed by the Rh(I) and the Ir(I)[27] complexes is the same within experimental error, the *induction periods* and the *rates of hydrogen consumption* are drastically different. Hydrogen uptake by the Ir complex $[(1,5\text{-COD})Ir{\cdot}P_2W_{15}Nb_3O_{62}]^{8-}$ begins after an induction period of only about 30 min in propylene carbonate and then proceeds with a pressure loss of 16×10^{-2} Torr/min. On the other hand, hydrogen uptake by the Rh(0) complex **1** in propylene carbonate has an ca. 8-fold longer induction period of 4 h. These results match the expectation that third row transition metals should nucleate faster than second row metals, due to their higher M−M bond dissociation energies and thus larger $M(0)_n$ critical nucleus cohesive bond energy (i.e., 159 kcal/mol for Ir−Ir vs 133 kcal/mol for Rh−Rh bonds, at least in the bulk metal[28]). However, after the longer induction period, the Rh(0) nanocluster catalyst proceeds with a pressure loss of 370×10^{-2} Torr/min—more than 20 times faster than Ir(0). This result matches the finding that second row transition metals tend, in general, to be faster catalysts for hydrogenation and other reactions.

Demonstration of an Overall Negative Charge on the Rh(0) Nanoclusters: Ion-Exchange Chromatography. Previously we used ion-exchange chromatography and electrophoresis to show that polyoxoanion-stabilized Ir(0) nanoclusters possess an overall negative charge due to the polyoxoanion binding to the Ir(0) nanocluster surface.[3] In the Ir(0) nanocluster work it was shown that *n* Ir(I) are reduced to neutral $Ir(0)_n$, [3.5 equiv of H_2/equiv $(1,5\text{-COD})Ir{\cdot}P_2W_{15}Nb_3O_{62}^{8-}$ precursor; recall Scheme 1], yet the resultant neutral $Ir(0)_n$ core nanoclusters bind to an anion-exchange resin in the Cl^- form, $P{-}NR_3^+Cl^-$, (P = Amberlyst A-27), but pass unimpeded down a cation-exchange resin, $P{-}SO_3^-$-Bu_4N^+, (P = Amberlite IRA-400 resin).[3b] Since no anions other than the $P_2W_{15}Nb_3O_{62}^{9-}$ polyoxoanion (plus its Nb−O−Nb bridged anhydride[3]) were present, the observation of overall anionically charged nanoclusters provides compelling evidence for the adsorption of the (anionic) polyoxoanion to the (neutral) $Ir(0)_{\sim 900}$ nanocluster surface.[3]

Herein, the same cation- and anion-exchange experiments were performed with $Rh(0)_{\sim 2400}$ nanoclusters to show, similarly, that the neutral $Rh(0)_{\sim 2400}$ core nanoclusters also bear an overall negative charge—*a negative charge that must, again, be due to the adsorption of the polyoxoanion to the Rh(0) nanocluster's surface.* Specifically, an amber acetonitrile solution of $Rh(0)_{\sim 2400}$ nanoclusters passed unimpeded down a cation-exchange column (Biorad AG50W-X2) in the Bu_4N^+ form ($P{-}SO_3^-$-Bu_4N^+, P = macroreticular polymer) without a change in color. (The amber band remained visible as it passed through the column and the color of the resin remained bright orange.) A TEM image of the amber-colored effluent that was collected showed unchanged Rh(0) nanoclusters (Figure E, Supporting Information). However, when the same acetonitrile solution of $Rh(0)_{\sim 2400}$ nanoclusters was passed down an anion-exchange column (Amberlyst A-27) in the Cl^- form ($P{-}NR_3^+Cl^-$, P = macroreticular polymer), the amber color remained on the column and only a colorless effluent was collected. A TEM image showed that no Rh(0) nanoclusters or bulk Rh(0) metal was present in the effluent.

(27) (a) In addition, the consumption of 3.5 equiv of H_2 by **1** in propylene carbonate within experimental error (3.9 ± 0.4 equiv) is in agreement with our published results for the formation of the analogous Ir(0) nanoclusters from the corresponding Ir complex, $[(1,5\text{-COD})Ir{\cdot}P_2W_{15}Nb_3O_{62}]^{8-}$ (3.5 ± 0.3 equiv of H_2 consumed in acetone).[7b] As a control and in order to make a direct comparison, the Ir(0) experiment was repeated herein but with the same solvent (propylene carbonate) and under other conditions (i.e., 9 mM $[(1,5\text{-COD})Ir{\cdot}P_2W_{15}Nb_3O_{62}]^{8-}$) used for the uptake experiment beginning with the Rh precatalyst **1**. As expected, the Ir complex again consumed 3.6 ± 0.4 equiv of H_2 (Figure D, Supporting Information). (b) In the current study, H_2 gas-uptake experiments with **1** or $[(1,5\text{-COD})Ir{\cdot}P_2W_{15}Nb_3O_{62}]^{8-}$ that are performed in acetone or acetonitrile consume hydrogen beyond the expected 3.5 equiv due to *hydrogenation of the solvent* by the resulting Rh(0) or Ir(0) nanoclusters (to isopropanol and ethylamine, respectively, as detected by GLC or ^1H NMR), Table A, Supporting Information. In our previous work,[3] H_2 gas-uptake experiments with $[(1,5\text{-COD})Ir{\cdot}P_2W_{15}Nb_3O_{62}]^{8-}$ in acetone gave only 3.5 ± 0.3 equiv of hydrogen, and did not exhibit any detectable further hydrogen consumption; however, the lower precision of the hydrogen pressure data in our previous work did not allow us to detect this slow, solvent hydrogenation reaction. The present work, employing a more sensitive hydrogen gas-uptake system, Figure I, Supporting Information, generates more precise data (±0.1 Torr) and, hence, detects the additional hydrogen uptake reported herein.

(28) Porterfield, W. W. *Inorganic Chemistry*; Addison-Wesley Publishing: Reading, MA, 1983; p 84.

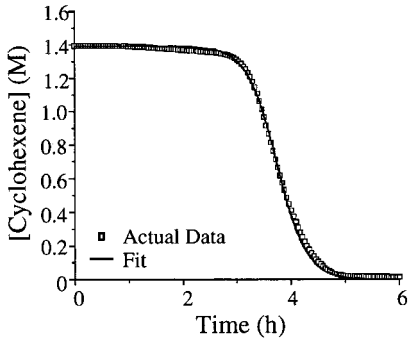

Figure 6. Curve fit of hydrogen pressure vs time beginning with $[(n\text{-}C_4H_9)_4N]_5Na_3[(1,5\text{-COD})Rh{\cdot}P_2W_{15}Nb_3O_{62}]$. The squares show the ± 0.01 psig data points, while the solid line indicates the corresponding excellent fit to those points. The calculated $k_{1(\text{hydrogenation})}$ value is $(3.7 \pm 0.7) \times 10^{-6}$ h^{-1}, and the stoichiometry and statistical factor corrected[5] $k_{2(\text{hydrogenation}),\text{corrected}}$ is $(4.7 \pm 0.1) \times 10^3$ M^{-1} h^{-1}.

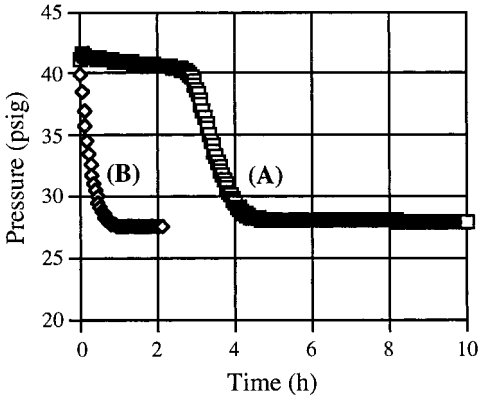

Figure 7. Comparison of cyclohexene hydrogenation beginning (A) from **1** under standard conditions, and (B) from the isolated Rh nanoclusters that result. In part A, the reaction proceeded after a 2.6 h induction period at a rate $-d[H_2]/dt =$ 2.6 mmol of H_2/h. In part B when the isolated nanoclusters were used, the reaction proceeds with no induction period and at a rate $[-d[H_2]/dt]_i = 8.1$ mmol of H_2/h.

These ion-exchange resin results demonstrate that the $Rh(0)_{\sim 2400}$ nanoclusters possess an overall negative charge, an indication that the highly negatively charged polyoxoanion is, as before,[3] a crucial factor in stabilizing the Rh(0) nanoclusters in solution.

Quantitative Kinetic Evidence Demonstrating that Rh(0) Nanoclusters Are Formed by Slow, Continuous Nucleation Followed by Autocatalytic Surface Growth. Figure 6 shows (i) a typical sigmoidal-shaped curve of hydrogen pressure loss vs time during the formation of $Rh(0)_{\sim 2400}$ nanoclusters and (ii) the corresponding fit to the data by the analytic kinetic equation provided elsewhere for the previously elucidated[5] A → B nucleation (rate constant k_1), and A + B → 2B autocatalytic surface growth (rate constant k_2) mechanism of transition-metal nanocluster formation under H_2. The calculated $k_{1(\text{hydrogenation})}$ and $k_{2(\text{hydrogenation}),\text{corrected}}$ values[5] from this fit are $(3.7 \pm 0.7) \times 10^{-6}$ h^{-1} and $(4.7 \pm 0.1) \times 10^3$ M^{-1} h^{-1}, respectively. (See the Experimental Section and elsewhere[5] for a description of the mathematically required "stoichiometry" and "scaling" correction factors to $k_{2(\text{hydrogenation}),\text{corrected}}$ that have been applied.) The excellent agreement between the observed kinetic data and the analytical fit—some of the best fits we have seen[5]—offers *prima facia* evidence that the nucleation, then autocatalytic surface growth, mechanism uncovered in our earlier study of $Ir(0)_{\sim 300}$ nanocluster formation[5] also applies in this case. Worth noting is that the separation in time of nanocluster nucleation from its growth, a feature required to obtain near-monodisperse particles, is a basic component of autocatalytic surface growth leading to the sigmoidal curves seen in Figures 6 and 7 for this $Rh(0)_{\sim 2400}$ system, just as was seen previously for the $Ir(0)_{\sim 300}$ nanoclusters.[5]

Comparison of k_1 (Nucleation) and k_2 (Growth) Rate Constants for Rh(0) vs Ir(0) Nanoclusters. We quantitated the rate constants for nanocluster nucleation (k_1) and growth (k_2) for the $Rh(0)_{\sim 2400}$ nanoclusters since (i) there is no prior, direct comparison of nanocluster nucleation and growth rate constants in the literature for different metals,[5,29] and (ii) it is of further interest to compare the $R' = k_2/k_1$ ratio (i.e., the ratio of growth to nucleation rate constants) for the 40 ± 6 Å $Rh(0)_{\sim 2400}$ and the 20 ± 3 Å $Ir(0)_{\sim 300}$ nanoclusters *grown under identical conditions*, since R' has been shown to reliably predict nanocluster size, at least for Ir(0) nanoclusters.[7]

The k_1 rate constant describing nanocluster nucleation, $k_{1(\text{hydrogenation})}$, is $(3.7 \pm 0.7) \times 10^{-6}$ h^{-1} for the formation of Rh(0) nanoclusters under Standard Conditions (see Experimental Section); for the analogous Ir(0) nanoclusters $k_{1(\text{hydrogenation})}$ is $(1.8 \pm 0.2) \times 10^{-3}$ h^{-1}. The Rh(0) value is *ca. 3 orders of magnitude smaller* than the value for Ir(0), indicating a substantially slower nucleation process in the Rh(0) example. A close look at our Rh(0) vs Ir(0) nanocluster size data, in combination with other nanocluster size data available in the literature,[15] suggests that nucleation may be largely controlled by the metal's $\Delta H_{(\text{vaporization})}$ value and thus M−M bond dissociation energy, an idea we are pursuing further and will report more on in due course.

The $k_{2(\text{hydrogenation}),\text{corrected}}$ rate constant for Rh(0) nanocluster growth under Standard Conditions is $(4.7 \pm 0.1) \times 10^3$ M^{-1} h^{-1}. The "corrected" subscript refers to two mathematically required correction factors, one of which corrects for the changing surface area of the growing nanocluster and, thus, for the difference in exposed surface areas of the larger (and thus lower surface area) Rh(0) vs smaller Ir(0) nanoclusters. (The Experimental Section and our earlier publication[5] contain additional details for the interested reader.) Note that the Rh(0) $k_{2(\text{hydrogenation}),\text{corrected}}$ value is ca. 2.1 larger than the $(2.2 \pm 0.3) \times 10^3$ M^{-1} h^{-1} value previously determined for Ir(0) nanocluster growth, also under standard conditions.[5] As expected, the larger $k_{2(\text{hydrogenation}),\text{corrected}}$ value for Rh(0) is consistent with the expectation that the k_2 (hydrogenative growth) rate constant for second row transition metals will be larger than that for their third row counterparts. The larger growth rates for the Rh(0) nanoclusters, in combination with the smaller nucleation rates, give rise to a larger k_2/k_1 value, or R' ratio, 1.3×10^9 for Rh(0) vs 1.2×10^6 for Ir(0), fully consistent with the finding that the ∼40 Å Rh(0) nanoclusters are larger in diameter than the ∼20 Å

(29) A New Kinetic Method to Follow Transition Metal Nanocluster Formation Based on Catalytic Activity and the Pseudoelementary Step Concept. Watzky, M. A.; Aiken, J. D., III; Widegren, J. A.; Finke, R. G., manuscript in revision.

Ir(0) nanoclusters, even when the nanoclusters are grown under otherwise identical conditions.

Isolation and Reuse of Rhodium Nanoclusters in a Cyclohexene Hydrogenation Reaction. As previously noted,[5] the close fit to our A → B and A + B → 2B kinetic scheme provides compelling kinetic evidence that A (i.e., the complex **1**) is *not* a catalyst at all (to within the ±15% experimental error of the fits) but that B is (B being the Rh(0) nanoclusters). Additional evidence confirming that the $Rh(0)_{\sim 2400}$ nanoclusters are indeed the true catalysts is provided by parts A and B of Figure 7 showing two hydrogen pressure vs time cyclohexene hydrogenation reactions under Standard Conditions, but beginning with the precatalyst **1** (curve A) vs beginning with the *isolated* $Rh(0)_{\sim 2400}$ nanoclusters (curve B). Curve A shows the expected induction period, after which cyclohexene hydrogenation proceeds with a rate $-d[H_2]/dt$ of 2.6 mmol of H_2/h. Once the precatalyst had been completely converted into active nanoclusters, the $Rh(0)_{\sim 2400}$ nanoclusters were isolated, resuspended in fresh acetone, and recharged with fresh cyclohexene substrate, and a second Standard Conditions hydrogenation experiment was initiated, curve B (see the Experimental Section for details). This reaction proceeded *without* an induction period and at an initial rate $[-d[H_2]/dt]_i$ of 8.1 mmol of H_2/h. The increase in the observed hydrogenation rate (as seen previously for Ir; see Table 2 in ref 4) going from the precatalyst to the isolated $Rh(0)_{\sim 2400}$, plus the lack of an induction period, are the expected results when Rh(0) nanoclusters, but not the precursor **1**, are the true catalysts.

Mercury Poisoning Experiments. Mercury is a well-known, accepted heterogeneous catalyst poison due to its adsorption on the catalyst surface and amalgam formation;[30] as a single test it is one of the fastest and more reliable (albeit not infalliable[11c]) tests for distinguishing "heterogeneous" (e.g., nanoclusters) from "homogeneous" (e.g., single metal) catalysts.[11c] In addition, we previously developed and successfully applied a series of mercury poisoning experiments which (i) poisoned authentic, well-characterized Ir(0) nanoclusters[4] and (ii) allowed the detection of Rh(0) nanoclusters in an arene hydrogenation system, one previously believed to involve a discrete, homogeneous $RhCl_4^-$ species as the catalyst.[11c]

Three types of Hg(0) poisoning experiments were done as part of the present studies to confirm that the Rh(0) nanoclusters are the active hydrogenation catalyst. First, a clear yellow solution of the precatalyst **1** was treated for 2 h by vigorous stirring with 4.0×10^3 equivalents of mercury (the excess has been shown elsewhere[11c] to be necessary to ensure that *all* the catalyst contacts Hg(0)). Once the excess mercury was removed by filtration, cyclohexene was added to the resulting clear yellow solution (now slightly lighter in color following the Hg(0) treatment) and active Rh(0) nanoclusters with full catalytic activity ($-d[H_2]/dt = 2.0$ mmol of H_2/h, Supporting Information, Figure F) were found to evolve after an increased induction period (10.5 hours, ca. 4-fold longer than the usual 2.5 ± 0.5 h induction period, but consistent with our earlier results[3] with Ir(0), in which the induction period was lengthened ca. 2-fold, from 2 to 4 h, after pretreatment of the precatalyst with Hg(0)). Note that these (and also our earlier[4]) experiments show the dramatic effect of trace, residual Hg(0) poisoning the low level of critical $Rh(0)_n$ nuclei formed in the nanocluster nucleation step.[5]

In a second Hg(0) poisoning experiment, a cyclohexene hydrogenation experiment involving active Rh(0) nanoclusters was stopped after ca. 50% conversion of cyclohexene and 4.3×10^3 equiv of mercury was added to the yellow solution and stirred vigorously for 1 h. Once the excess Hg(0) was removed by filtration, the now faint-yellow (instead of yellow/amber) solution was reattached to the hydrogenation line. *No additional catalytic activity was observed even after 18 h* (Supporting Information, Figure G). Finally, 4.0×10^3 equiv of Hg was added to a solution of the precatalyst **1** and a standard conditions hydrogenation experiment was started. No catalytic activity was observed, even after 22 h, or nearly ten times the normal 2.5 h induction period (Supporting Information, Figure H).

These Hg poisoning experiments show that treatment of a solution of either active, or forming, Rh(0) nanoclusters *completely suppresses all catalytic activity within experimental error (±5%)*. These Hg poisoning experiments are, then, additional strong evidence that the Rh(0) nanoclusters are the true catalysts in this system.

Investigation of the Infrequent Variability in Observed Rates Beginning with 1. As first reported elsewhere,[31] the initial out of six total batches of the Rh precatalyst complex **1** prepared throughout this study showed ca. 5-6 fold faster catalytic hydrogenation rates (i.e., >15 mmol H_2/h), under otherwise identical standard conditions, compared to the rates reported herein for the other five, subsequent batches of precatalyst **1**. This is despite the fact that we find that the reproducibility of the rates *within* each batch of Rh precursor **1** is the expected 15−20%, as we have seen previously for Ir.[3,4] In the Supporting Information, we consider and rule out all of the possible sources of this variability that we could conceive of [trace O_2, trace H_2O, trace Br^- left over from the n-$Bu_4N^+Br^-$ used in the synthesis, inhomogeneous (and thus variable) nucleation, or the hydrogenation apparatus itself]. Noteworthy here is that two of the batches of **1** used herein were actually made by two other, independent researchers, yet those two batches of **1** still give hydrogenation rates *reproducible* to ≤±15−20% *inter*batch. Hence, the first batch of **1** is presently an "outlier", but we still felt it was important to mention this (infrequent) result. We conclude that the infrequent rate variability is intrinsic to that first, particular batch of **1** itself which we believe, in turn, *indicates the need to follow the detailed synthesis of* $P_2W_{15}Nb_3O_{62}^{9-}$ *and* ***1*** *exactly*.[10ab,32a]

However, another explanation merits mention. The TEM data in Figure 3 (of one of the five, reproducible rate, slower activity batches of Rh(0) nanoclusters)

(30) (a) Georgiades, G. C.; Sermon, P. A. *J. Chem. Soc. Chem. Commun.* **1985**, 975. (b) Whitesides, G. M.; Hackett, M.; Brainard, R. L.; Lavalleye, J.-P. P. M.; Sowinski, A. F.; Izumi, A. N.; Moore, S. S.; Brown, D. W.; Staudt, E. M. *Organometallics* **1985**, *4*, 1819. (c) Moyes, R. B.; Wells, P. B. *Adv. Catal.* **1973**, *23*, 121.

(31) Elsewhere we reported that two of seven batches of **1** give high rates.[12] However, we now know that the first batch of **1** that gave a high rate utilized a batch of $P_2W_{15}Nb_3O_{62}^{9-}$ precursor that was synthesized by a new postdoctoral fellow who was just learning the synthesis of **1** and whom we now know did not follow every step of the synthesis exactly as described in detail. This, again, emphasizes the need to follow *every step* of the synthesis in the synthetic paper of **1** exactly as described.[10] (There are also two typographical errors in the synthetic paper elsewhere[32] that one should note.)

shows that ~8% of the particles are triangular (vs spherical), so that this particle geometry (and associated active sites, for example the {111} vs {100} faces on a cubic close packed Rh(0) nanoparticle,[6] and their intrinsically different catalytic rates[6]) are other possible sources of this variability. In one sense, it is remarkable that the 15−20% *intra*-batch catalytic reproducibility of **1**, and the only once to date 5−6 fold *inter*-batch variability of the catalytic rate, can be obtained in a reaction whose average stoichiometry is ~2400 **1** → $Rh(0)_{\sim 2400}$ and thus must involve >2400 mechanistic steps (as discussed elsewhere[5]).

At this time, several points seem clear: (i) although rarely done, it is important (as done herein, and as done previously for our Ir(0) nanoclusters[3,4]) to report both the intra- and interbatch reproducibility in the catalytic activity and other properties of nanoclusters; (ii) the $Ir(0)_{\sim 300}$ nanocluster catalytic data reported elsewhere proves that ±15−20% intra- *and* interbatch reproducibility is achievable for at least some transition metals using appropriate, well-characterized, reproducible precursors (i.e., $[(1,5\text{-COD})Ir{\cdot}P_2W_{15}Nb_3O_{62}]^{8-}$ in that case); (iii) the precursor to the Rh(0) nanoclusters, **1**, appears to be the source of the variability in the present case, but only one time out of six syntheses (complex **1** is known to exist as ≥2 isomers, in contrast to the related $[(1,5\text{-COD})Ir{\cdot}P_2W_{15}Nb_3O_{62}]^{8-}$, which exists as a single isomer only,[10b] so this is another possible source of the infrequent variability).

The important implications, then, are that for at least some transition metals, the resultant nanocluster catalytic activity and reproducibility may be more highly dependent on the exact composition, purity, and structure (e.g., isomers?) of the nanocluster precursor than previously appreciated. These are certainly points worthy of future experimental scrutiny and investigation. Note that the evidence to date is that the $[(1,5\text{-COD})M^{n+}{\cdot}P_2W_{15}Nb_3O_{62}]^{8-}$ precursors are, actually, among the few nanocluster precursors *proven* to give catalytic activity that is generally *reproducible* to ±15−20%. The data for the M^{n+} = Ir(I) case is especially compelling; in probably >200 individual $Ir(0)_{\sim 300}$ nanocluster formation reactions from six different researchers, over a ≥8 year time period, and from probably at least 30 individual syntheses and batches of precatalyst, the ±15−20% catalytic reproducibility has invariably been seen in our standard test reaction of cyclohexene hydrogenation.

Summary

To summarize, the work reported herein shows the following.

(1) Near-monodisperse 40 ± 6 Å $Rh(0)_{\sim 1500}$ to $Rh(0)_{\sim 3700}$ nanoclusters can be prepared by the reduction, in acetone and under H_2, of $[(n\text{-}C_4H_9)_4N]_5Na_3[(1,5\text{-COD})Rh{\cdot}P_2W_{15}Nb_3O_{62}]$ and in the presence of cyclohexene, undergoing hydrogenation to cyclohexane. The resultant $Rh(0)_{\sim 2400}$ nanoclusters are sufficiently stable to be isolable as a black powder which can then be fully redissolved in solution.

(2) The $Rh(0)_{\sim 1500}$ to $Rh(0)_{\sim 3700}$ nanoclusters have been characterized by TEM, EDS (confirming the presence of Rh and the $P_2W_{15}Nb_3O_{62}^{9-}$ polyoxoanion), electron diffraction (confirming the ccp Rh(0) metal core), UV−visible spectroscopy, and elemental analysis and have an *average* formula $[Rh_{\sim 7}(P_4W_{30}Nb_6O_{123})TBA_{\sim 5.5}\text{-}Na_{\sim 10.5}]_{\sim 340}$.

(3) The hydrogen pressure vs time curves during the nanocluster formation reaction are quantitatively fit by our previously established mechanism[5] consisting of slow nucleation (k_1), followed by fast autocatalytic surface growth (k_2).

(4) The $k_{2(\text{hydrogenation}),\text{corrected}}$ for polyoxoanion-stabilized Rh(0) nanoclusters is larger by ca. 2.1 fold than the analogous Ir(0) value.

(5) The nanoclusters possess an overall negative charge in solution, as demonstrated by ion-exchange chromatography, an observation requiring that the anionic $P_2W_{15}Nb_3O_{62}^{9-}$ polyoxoanion binds to the electron deficient surface of the Rh(0) nanoclusters.

(6) Treatment of either forming, or fully formed, Rh(0) nanoclusters with Hg(0) completely suppresses all catalytic activity within experimental error (±5%), thereby providing confirming evidence (i.e., along with the A → B, A + B → 2B kinetic evidence) that the nanoclusters ("B") are the true catalysts.

In other, completed work we have shown that the Rh(0) nanoclusters derived from **1** exhibit extremely long catalytic lifetimes in solution, ≥193 000 total turnovers, an unprecedented result for a nanocluster catalyst in solution.[1k] We have also undertaken CS_2 poisoning studies aimed at providing badly needed, quantitative data about the number of surface-active sites on nanocluster catalysts (see the comments elsewhere about this point[1k]). These studies, plus catalytic lifetime and activity comparisons to other Rh homogeneous and heterogeneous catalysts, will be reported elsewhere.[13]

Experimental Section

Materials. Cyclohexene (Aldrich, 99+%, stabilized with 0.01% 2,6-di-*tert*-butyl-4-methylphenol) was distilled from Na under argon immediately prior to use and stored in a Vacuum Atmospheres drybox (≥99% resultant purity by GLC). Acetone (Burdick and Jackson, 0.26% H_2O) was transferred into the drybox and purged for ≥30 min with nitrogen using a glass bubbler. The source, purity, and water content of the acetone are known to be crucial to obtaining reproducible kinetics of nanocluster formation and catalysis in these systems.[4] Hydrogen gas (General Air, 99.5%) used on the hydrogenation apparatus, Figure I, Supporting Information, was prepurified by passage through a moisture trap (Scott Specialty Gases, Baxter Scientific), an oxygen trap (R&D Separations type OT3, Baxter Scientific) and an indicating oxygen trap (R&D Separations, Hewlett Packard). Elemental mercury (D. F. Goldsmith Chemical & Metal Corp., elemental grade, triply distilled), cation-exchange resin (AG 50W-X2, 50-100 mesh, analytical grade, Biorad), and anion-exchange resin (Amberlyst A-27) were used as received. Methylcyclohexane (Aldrich) was degassed and stored in a drybox. The $[(n\text{-}C_4H_9)_4N]_9P_2W_{15}Nb_3O_{62}$ polyoxoanion used in the synthesis of **1** was synthesized according to our more recent procedure and its purity checked by ^{31}P NMR.[32] (As a further check of the purity of

(32) $P_2W_{15}Nb_3O_{62}^{9-}$ synthesis and characterization papers: (a) Weiner, H.; Aiken, J. D., III; Finke, R. G. *Inorg. Chem.* **1996**, *35*, 7905−7913 and references therein. Note that this manuscript has two typographical errors: p 7910, right-hand column, 12th line: "84% excess" should read "2% excess"; p 7910, footnote 20, 4th line: "5%" should read "0.5%". (b) Finke, R. G.; Lyon, D. K.; Nomiya, K.; Weakley, T. J. *Acta Crystallogr., Sect. C* **1990**, *46*, 1592. (c) Edlund, D. J.; Saxton, R. J.; Lyon, D. K.; Finke, R. G. *Organometallics* **1988**, *7*, 1692−1704.

$[(n\text{-}C_4H_9)_4N]_9P_2W_{15}Nb_3O_{62}$, the ^{31}P NMR titration with (1,5-COD)M$(CH_3CN)_2^+BF_4^-$ (M=Rh, Ir) shown elsewhere[32a] is recommended, and a break point of 1.0 ± 0.1 should be seen.) The air-sensitive polyoxoanion-supported organometallic precatalyst $[(n\text{-}C_4H_9)_4N]_5Na_3[(1,5\text{-COD})Rh{\cdot}P_2W_{15}Nb_3O_{62}]$, **1**, was synthesized as previously reported[10] and stored in a drybox. The purity of **1** was established by ^{31}P NMR and C, H, N analysis (Atlantic Microlabs). [Anal. (Calcd) Found: C, (18.93) 18.88; H, (3.47) 3.54; N, (1.25) 1.27].

Analytical Procedures. Unless otherwise reported all reaction solutions were prepared under oxygen- and moisture-free conditions using a Vacuum Atmospheres nitrogen drybox (<1 ppm O_2 as continuously monitored by a Vacuum Atmospheres O_2-level monitor).

Nanoclusters were examined by transmission electron microscopy using a JEOL TEM 2000 EX-II operating at an accelerating voltage of 100 keV. Samples were prepared using type A (300 mesh) formvar- and carbon-coated copper grids (supplier, Ted Pella). Grids were gently suspended in chloroform for about 30 s immediately prior to use to remove the formvar coating and to expose a fresh carbon surface. One drop of the nanocluster solution (at a concentration of ca. 1 mg/mL, in either acetone or acetonitrile) was placed on the carbon-coated grid using a gastight syringe and allowed to air dry. Samples were examined at magnifications between 100 and 400K, and in at least three different, random places on the sample grid to ensure that the images seen were representative of the sample as a whole. Reported magnifications are those of the original negative. Particle-size distributions were determined once the original negative had been digitally scanned into Adobe Photoshop and expanded to >20 in. × 25 in. for easier size measurement and resolution. Control experiments showed that a solution of the rhodium-containing nanocluster precursor complex **1** does not form nanoclusters under TEM conditions identical to those used to examine authentic nanocluster samples (Supporting Information, Figure J). [Previously reported control experiments[3] also showed that *iridium* nanocluster samples are not perturbed by changing either electron beam accelerating voltage (40 or 100 keV), or by varying sample exposure times under the beam (seconds *vs* minutes).]

Samples were analyzed by energy dispersive X-ray spectroscopy (EDS) on the JEOL TEM using a Kevex Super 8000, running Quantex Version 6.0, coupled to a Quantum thin window detector (mylar window; 30 mm^2 detector area with a resolution of 116 eV at 1.49 keV). Electron beam spot sizes (typical instrument settings of between 2 and 5) were adjusted so that events occurred with a deadtime of ≤ 50% at between 1000 and 2000 counts/s. The instrument was calibrated to the K lines of Al and Cu; peak assignments are based on X-ray emission wavelengths and intensities in Quantex.

Electron diffraction was performed on a Philips CM-12 TEM using an accelerating voltage of 100 keV and a camera length of 770 mm. Diameters of the diffraction rings obtained were measured to the nearest 0.5 mm, and *d*-spacings were calculated using the equation $dr = l\lambda$ where *d* is the *d*-spacing in Å, *r* is the radius of the diffraction rings in mm, *l* is the camera length in mm, and λ is the wavelength of the electrons in Å (0.037 Å at 100 keV[33]). As a control, and to ensure proper calibration, an evaporated gold sample was used as a standard and examined immediately prior to examination of the Rh(0) nanoclusters at the identical camera length and accelerating voltage. The *d*-spacings of the sputtered Au sample were found to match the literature *d*-spacings of an Au(0) control sample, literature[17] (vs found, in Å) [assigned Miller indices]: 2.36 (2.36) [111]; 2.05 (2.04) [200]; 1.46 (1.44) [220]; 1.29 (1.23) [311]; 0.94 (0.95) [331]. To overcome errors introduced into the camera constant $l\lambda$ (and, hence, in the *d*-spacings) caused by voltage fluctuations or any error in the apparent camera length, the ratio of each ring diameter relative to the center-most ring radius was calculated as described by the equation[33] $r_{outer}/r_{inner} = d_{inner}/d_{outer}$. These values were then matched to the known Rh(0) or Au(0) *d*-spacings. Rh(0) sample *d*-spacing values in Å, literature[17] (vs found) [Miller indexed line]: 1.35 (1.35) [220]; 1.15 (1.15) [311]; 0.85 (0.85) [420].

Hydrogen gas-uptake experiments during Rh(0) nanocluster formation were performed in the general manner previously described.[3] The uptake apparatus (Figure K, Supporting Information) is composed of the following major pieces: a high vacuum line ($\leq 10^{-4}$ Torr, as continuously measured by a Varian 524-2 Cold Cathode Gauge); a Pyrex reaction bulb of a known volume (V_{flask} = 51.25 mL; V_{arm} = 5.63 mL); a MKS Type 122A Baratron pressure transducer (+999 Torr max) of a known volume ($V_{Baratron}$ = 21.02 mL); a 500 mL water-jacketed reaction vessel (Chemglass).

Gas-liquid chromatography (GLC) of the hydrogenation product cyclooctane was performed using a Hewlett-Packard 5890 Series II GC with a FID detector equipped with a 30 m (0.25 mm i.d., 25 μm film) Dowex DB-1 column and coupled to a Hewlett-Packard 3395 integrator. Parameters were as follows: initial temperature, 50 °C; initial time, 3 min; ramp, 10 °C/min; final temperature, 160 °C; final time, 16 min; injector port temperature, 180 °C; detector temperature, 200 °C; injection volume, 4 μL.

UV−visible spectroscopy was performed using a Hewlett-Packard 8452A diode array spectrophotometer.

Hydrogenation Experiments (Standard Conditions) and Calculation of Reaction Rates. Hydrogenation reactions were performed using our previously described pressurized hydrogenation apparatus[4] (Figure I, Supporting Information) except that it was equipped with an improved pyrex water-jacketed reaction flask (200 mL; supplier, Andrews Glass Company). Briefly, this apparatus consists of a Fischer-Porter bottle attached to both a H_2 source and a pressure transducer via two separate Swagelock TFE-sealed Quick-Connects. Hydrogen pressure in the Fischer-Porter bottle was continuously monitored using the computer-interfaced pressure transducer (Figure I, Supporting Information) and an Omega Model PX621 pressure transducer attached to an 486/66 PC via an Omega WB35 A/D converter; the pressure vs time data was processed using Microsoft Excel. *All reaction mixtures were prepared in the drybox*. The protocol which follows parallels that which we used earlier.[3,4] In each experiment, the precursor **1** was weighed into a 1 dram vial and dissolved in 2.5 mL acetone, added via a 10 mL gastight syringe, to yield a clear, bright yellow solution. Cyclohexene (0.5 mL, 1.65 M) was added and the resultant clear, homogeneous solution was transferred via polyethylene pipet into a fresh 22 × 175 mm borosilicate culture tube containing a new $^5/_{16}$ in. × $^5/_8$ in. Teflon-coated magnetic stir bar. The culture tube was then sealed inside of the Fischer-Porter pressure bottle that is part of the hydrogenation apparatus; the Fischer-Porter bottle was brought outside of the drybox and placed inside a constant temperature circulating water bath (VWR Scientific, 22.0 ± 0.1 °C). Next, the hydrogenation line was evacuated for at least 1 h, to remove any trace oxygen and water present, and then the line was refilled with purified hydrogen. The Fischer-Porter bottle was then attached to the hydrogenation line via its TFE-sealed Swagelock Quick-Connects, and the bottle was then purged 15 times with hydrogen (15 s per purge, with stirring) and stirred vigorously for an additional 2 min, and $t = 0$ was noted.

Reaction rates were calculated from the rate of hydrogen pressure loss ($-d[H_2]/dt$, expressed in mmol H_2/h) as determined by the slope of the linear portion of the H_2 uptake curve, an example of which is shown in Figure 2. As demonstrated elsewhere[5] this slope correlates linearly with the bimolecular rate constant k_2 for nanocluster autocatalytic surface growth (i.e., and not for the cyclohexene hydrogenation reaction; see ref 5). The rate constant (k_2) was obtained when desired as before, by quantitative curve-fitting of the hydrogen pressure vs time data to the appropriate nucleation (k_1) plus autocatalytic surface-growth (k_2) kinetic expressions.[5]

Synthesis of Near-Monodisperse 40 ± 6 Å Rh Nanoclusters Beginning from the Polyoxoanion-Supported Precatalyst 1. In a drybox, **1** (20.1 mg, 3.6×10^{-3} mmol) was

(33) Thomas, G.; Goringe, M. J. *Transmission Electron Microscopy of Materials*; John Wiley and Sons: New York, 1979.

dissolved in 2.5 mL of acetone in a disposable glass dram vial to yield a bright, clear-yellow solution. Cyclohexene was added (0.5 mL, 1.65 M) and the clear-yellow reaction solution was transferred via a disposable polyethylene pipet into a fresh borosilicate culture tube containing a $^5/_{16}$ in. × $^5/_8$ in. Teflon-coated magnetic stir bar and sealed in the Quick-Connects fitted Fischer-Porter bottle, which was brought out of the drybox and attached to the hydrogenation line. A standard conditions hydrogenation reaction (22 °C, 40 ± 1 psig H_2) was then started, all as detailed in the "Hydrogenation Experiments (Standard Conditions)" section above. As the reaction proceeded, the original clear yellow solution became turbid and dark yellow/amber. After 13.5 h (to allow complete conversion of the precatalyst **1** into nanoclusters) the nanoclusters were isolated as described below.

Nanocluster Sample Isolation and Preparation for TEM Analysis. The Rh(0) nanocluster isolation procedure parallels that which we used previously for our Ir(0) nanoclusters.[4] After 13.5 h the Fischer-Porter bottle containing the reaction solution was disconnected from the hydrogenation line via the Quick-Connects and taken back into the drybox, the hydrogen pressure was released, and the turbid nanocluster solution was poured into a 1 dram vial and tightly capped with a plastic snap cap. The turbid solution was then allowed to stand undisturbed in the drybox for ≥10 h, after which time the nanoclusters had settled as a black precipitate. The supernatant was carefully removed via a polyethylene pipet and discarded. While still in the drybox, the black nanocluster precipitate (now in ≤0.5 mL of solution) was dried under vacuum overnight at room temperature to yield 2.7 mg of a black powder. Elemental analyses (Galbraith Laboratories, samples handled under N_2 and combusted with V_2O_5) were performed on four different samples. The average values for C, H, and N (determined for all four samples, including a repeat analysis on two of those samples) are provided in Table A of the Supporting Information. Anal. Calcd for $[Rh_7(P_4W_{30}Nb_6O_{123})TBA_{5.5}Na_{10.5}]_x$ (found, averages): C, 10.10 (10.45); H, 1.91 (2.51); N, 0.74 (1.34); Rh, 6.89 (7.32); P, 1.18 (1.03). The reasons for the observed differences between the calculated and found values (especially for N) are discussed in the Supporting Information.

A TEM sample was prepared by redissolving the 2.7 mg of black powder in 3 mL of fresh acetonitrile to yield a clear, amber, homogeneous solution (no bulk metal was visible by the naked eye at any time). A drop of this solution was then dispersed on a TEM grid.

GLC Determination of the Evolved Equivalents of Cyclooctane vs Time During Rh Nanocluster Formation. In the drybox, methylcyclohexane (4 μL; as a GLC internal standard) was added using a 5 μL gastight syringe to a clear, bright-yellow solution of **1** (20.9 mg, 3.7×10^{-3} mmol, 1.2 mM) dissolved in 2.5 mL of acetone and 0.5 mL of cyclohexene in a disposable glass dram vial. A standard conditions hydrogenation reaction was then started in the usual fashion. At the prechosen times indicated by the data in Figure 2, the hydrogen pressure was released and aliquots (≤0.1 mL) of the reaction solution were drawn using an 18 in., thoroughly H_2-purged needle attached to a gastight syringe that had been inserted through the ball valve at the top of the Fischer-Porter bottle, all while under a continuous flow of one atm of H_2. Once the aliquot was taken, the Fischer-Porter bottle was purged an additional five times (15 s per purge) with hydrogen gas and resealed at 40 psig H_2. The production of cyclooctane *vs* time is summarized in Figure 2 (right axis). Note that these experiments are at a nearly constant 40 psig H_2 pressure and thus differ slightly from the average 34 ± 6 psig H_2 under a standard conditions hydrogenation reaction that consumes all of the added cyclohexene.[34]

(34) See also footnote 37 in ref 5, which describes how, as a needed practical assumption, the treatment of the H_2 pressure in our "Standard Conditions" experiment as a "constant" 34 ± 6 psig H_2 (i.e., spanning the 40 to ca 28 psig H_2 pressure drop) introduces only a quite tolerable ca. 17% error into the final k_1 and k_2 rate constants.

Quantitative Curve-Fitting of Cyclooctane Equivalents vs Time Data. Curvefitting of hydrogen pressure or cyclooctane equivalents vs time was performed as described before[5] except using the software package Microcal Origin 3.54. [Origin is also a nonlinear regression subroutine (RLIN) and uses the same modified Levenberg−Macquard algorithm as described previously.[5]] As a control experiment to assure that the reported values of k_1 and k_2 are accurate, a mock set of data was calculated and then curve-fit consisting of time intervals every 2.5 min (as in the case of the hydrogen pressure vs time) and with $k_1 = 0.005$, $k_2 = 1.00$ and $[A]_0 = 1.2$. During fitting of the first 110 data points (i.e., up to 50% of the total pressure loss), Origin refound the initial supplied values of $k_1 = 0.005$ ($\pm 1 \times 10^{-4}$% error) and $k_2 = 1.00$ ($\pm 3 \times 10^{-5}$% error) to within the indicated errors, thereby demonstrating the fidelity of Origin for the present curve fits and in our hands.

Correction Factors for k_2. The values of k_2 reported herein were corrected by the mathematically required correction factors detailed elsewhere.[5] Both a stoichiometry and a scaling correction factor were used,[5] $k_{2(\text{hydrogenation}),\text{corrected}} = k_{2(\text{hydrogenation})}/0.8$ and $k_{2(\text{hydrogenation})} = k_{2(\text{hydrogenation}-\text{fit})} \times 1400$, that is $k_{2(\text{hydrogenation}),\text{corrected}} = k_{2(\text{hydrogenation}-\text{fit})} \times 1400/0.8$. (Complete details describing both stoichiometry and scaling factors are provided elsewhere for the interested reader.[5]) For hydrogenation-determined k_2 values, the scaling factor is $(1 + x_{\text{growth}})/2 = 0.8$ for a growing 2→3 shell number cluster, which is the estimated size of the nanoclusters over the time period of the hydrogenation fit.[5] For GLC-determined k_2 values the required scaling factor, $(1 + x_{\text{growth}})/2 = 0.6$, was used, $k_{2\text{GLC(corrected)}} = k_{2\text{GLC}-\text{fit}}/0.6$. (No stoichiometric factor is required for the GLC-determined k_2 value since the cyclohexene hydrogenation is not followed.) The fit of hydrogen pressure vs time is shown in Figure 4. The fit of the evolved equivalents of cyclooctane vs time during the synthesis of $Rh(0)_{\sim 2400}$ nanoclusters is provided as Figure L of the Supporting Information.

Isolation and Reuse of the Rh Nanoclusters as Cyclohexene Hydrogenation Catalysts. A Standard Conditions hydrogenation reaction was carried out beginning with **1** (20.1 mg, 3.6×10^{-3} mmol). Once the reaction was complete, the Fischer-Porter bottle containing the reaction mixture was taken back into the drybox and the hydrogen pressure was released through the ball valve on top of the vessel. The product solution was then evacuated for 2 h at room temperature (through the Fischer-Porter bottle ball valve as previously described) until all of the solvent was removed and a black-brown powder remained. The nanocluster powder in the culture tube was then redispersed in 2.5 mL acetone and 0.5 mL fresh cyclohexene to give an amber solution. (Some slight cloudiness is seen; a control experiment showed that filtration of this solution through Whatmann #4 filter paper prior to beginning the hydrogenation run did not affect the catalytic activity of the resulting nanocluster solution.) The Fischer-Porter bottle was then sealed and brought from the drybox, and a second hydrogenation run was started with this isolated nanocluster catalyst. This reaction proceeded without an induction period with a rate of $[-d[H_2]/dt]_i = 8.1$ mmol of H_2/h; the H_2 pressure vs time curves for both reactions are shown in Figure 7.

Demonstration that Rh(0) Nanoclusters Have an Overall Negative Charge: Ion-Exchange Chromatography. All ion-exchange column processes were performed using a 25 mL buret (11 mm in diameter) equipped with a stopcock and a glass-wool plug. Unless otherwise noted, the column was packed to ca. 9 cm height, corresponding to ca. 8.6 cm^3 of resin slurry. As a control, the previously established ion-exchange experiments described in our earlier paper,[3] and on the negatively-charged polyoxoanion stabilized $Ir(0)_{\sim 900}$ nanoclusters, were repeated herein with identical results to those published previously[3] (see Figure M and complete experimental details in the Supporting Information). Specifically, the $Ir(0)_{\sim 300}$·polyoxoanion nanoclusters were shown to adsorb strongly to an anion-exchange column in the Cl^- form, $P-NR_3^+Cl^-$, but pass unimpeded down a cation-exchange column in the $[Bu_4N]^+$ form, $P-SO_3^-Bu_4N^+$.

(1) Anion-Exchange Chromatography of Rh(0) Nanoclusters. In a drybox, anion exchange resin (Amberlyst A-27 in Cl^- form, $P-NR_3^+Cl^-$, P = macroreticular polymer, ca. 24 g, dry) was placed in a 50 mL beaker and washed for 1 h with 25 mL of acetonitrile by continuous stirring. The acetonitrile was decanted, and the resin slurry was packed onto the column. The packed resin was washed with additional acetonitrile until the effluent was clear and colorless. Then 1.5 mL of a clear, dark-amber acetonitrile solution of $Rh(0)_{\sim 2400}$ nanoclusters (ca. 1 mg/mL) was loaded on the column and allowed to pass down through the column at a rate of ca. 20 drops/min. A colorless effluent was collected, in which no Rh nanoclusters or bulk metal particles were observed by TEM. In addition, the top portion of the resin turned from cream colored to dark brown, an observation consistent with the (anionic) $[Rh(0)_{\sim 2400}\cdot(\text{polyoxoanion})_x{}^{n-}]$ nanoclusters being adsorbed onto the anion-exchange resin.

(2) Cation-Exchange Chromatography of Rh(0) Nanoclusters. Cation-exchange resin in the $[Bu_4N]^+$ form (Biorad, $P-SO_3^-Bu_4N^+$, P = macroreticular polymer, ca. 300 mL) was washed for 45 min in 1.0 L of house-distilled water. The resin material was packed onto a column and first washed with water until the pH of the effluent was 7 (measured by a pH meter) and then washed with 400 mL of 50/50 acetonitrile/water and finally with ca. 800 mL of acetonitrile to remove any water remaining in the resin. Approximately 125 mL of resin slurry was added to a 250 mL round bottomed flask, which was sealed with a septum and purged for 1 h with argon gas. The flask containing the argon-saturated resin was then transferred into the drybox and used to pack a column. Next, 1.5 mL of a clear, dark-amber acetonitrile solution of $Rh(0)_{\sim 2400}$ nanoclusters (ca. 1 mg/mL) was loaded on the column and allowed to pass down through the column at a rate of ca. 20 drops/min. The amber band remained visible as it passed through the column and the color of the resin remained bright-orange. The dark-amber effluent was collected and was shown by TEM to contain 40 Å $Rh(0)_{\sim 2400}$ nanoclusters similar to those imaged before the ion-exchange procedure (Supporting Information, Figure E).

Mercury Poisoning Experiments. (1) Cyclohexene Hydrogenation Using Mercury-Pretreated 1 as Precatalyst. In a drybox, 20.7 mg (3.71×10^{-3} mmol) **1** was weighed into a dram vial and dissolved in 2.5 mL of acetone to yield a clear, bright-yellow solution. Elemental mercury (a large excess; 3.006 g, 14.99 mmol, 4.0×10^3 equiv) was added to the solution, the dram vial was capped with a plastic snap cap, and the mixture was stirred vigorously for 2 h using a $^5/_{16}$ in. × $^5/_8$ in. Teflon-coated stir bar. The mixture was then filtered three times through Whatman #1 filter paper to collect the excess mercury, yielding a clear yellow solution. Cyclohexene (0.5 mL, 1.65 M) was added and the clear yellow solution was transferred into a fresh culture tube and sealed in a Fischer-Porter bottle which was brought from the drybox and attached to the hydrogenation line where a standard conditions hydrogenation reaction was started. A plot of H_2 pressure vs time reveals a 4-fold larger, 10.5-h induction period, but a still eventually active catalyst, Figure F, Supporting Information.

(2) Cyclohexene Hydrogenation Using Mercury-Treated Rh(0) Nanoclusters. In a drybox, **1** (19.7 mg, 3.53×10^{-3} mmol) was weighed into a dram vial and dissolved in 2.5 mL of acetone to yield a clear, bright-yellow solution. Cyclohexene (0.5 mL, 1.65 M) was added and the clear yellow solution was transferred into a fresh culture tube and sealed in a Fischer-Porter bottle, which was brought from the drybox and attached to the hydrogenation line where a standard conditions reaction was started. After ca. 50% of the cyclohexene had been hydrogenated, the hydrogenation reaction was stopped by shutting off the stirring. The Fischer-Porter bottle was disconnected from the hydrogenation line and transferred into the drybox. Once inside the drybox, the hydrogen pressure was released and the yellow reaction solution was poured into a 2 dram vial containing a $^5/_{16}$ in. × $^5/_8$ in. Teflon-coated stir bar. Elemental mercury (a large excess; 3.021 g, 15.06 mmol, 4.3×10^3 equiv) was added to the yellow solution, the vial was capped with a plastic snap cap, and the mixture was stirred vigorously for 1 h. The mixture was then filtered three times through Whatman #1 filter paper to collect the excess mercury, yielding a clear yellow solution. Cyclohexene (0.2 mL) was added to this clear yellow solution (to make up for the cyclohexene that had already been consumed) and it was transferred into a new culture tube containing a stir bar, placed inside of a Fischer-Porter bottle, brought from the drybox, and attached to the hydrogenation line where a standard conditions reaction was restarted. A plot of H_2 pressure vs time is shown in Figure G, Supporting Information, revealing that the previously active Rh(0) nanocluster catalysts had been completely poisoned by the Hg(0).

(3) Attempted Cyclohexene Hydrogenation in the Presence of Mercury Using the Precatalyst 1. In a drybox, **1** (21.1 mg, 3.78×10^{-3} mmol) was weighed into a dram vial and dissolved in 2.5 mL of acetone to yield a clear, bright yellow solution. Cyclohexene (0.5 mL, 1.65 M) was added. Elemental mercury (a large excess; 3.074 g, 15.33 mmol, 4.0×10^3 equiv) was added to the clear yellow solution and the mixture was transferred into a fresh culture tube and sealed in a Fischer-Porter bottle which was brought from the drybox and attached to the hydrogenation line where a "Standard Conditions" reaction was started. A plot of H_2 pressure vs time showed no catalytic activity was established, even after 20 h; see Figure H, Supporting Information.

H_2 Gas-Uptake Experiments Beginning with the Precatalyst 1. In a drybox, **1** (97.8 mg, 1.75×10^{-5} mol) was weighed into a 2 dram vial and dissolved in 2.0 mL of propylene carbonate (added via gastight syringe) to yield a clear orange-yellow solution. This solution was then transferred via disposable polyethylene pipet into a reaction bulb containing a 1 mm × 3 mm Teflon-coated magnetic stir bar. The reaction bulb was sealed, removed from the drybox, and clamped (using an ethylene-propylene O-ring) via its side arm to a vacuum line (Figure K, Supporting Information). Next, the reaction solution was completely degassed (i.e., to $<10^{-4}$ Torr) via two freeze−pump−thaw cycles at liquid nitrogen temperature. (Thawing was accomplished by submerging the reaction bulb in a plastic cup filled with warm water.) The reaction solution was then refrozen, and the reaction bulb containing the frozen reaction solution was evacuated and sealed (by closing stopcock 4, Figure K, Supporting Information) under vacuum. The vacuum line above the sealed reaction bulb (Figure K, Supporting Information) was then purged by a continuous flow of hydrogen for at least 10 min. The stopcock connecting the hydrogen tank to the vacuum line (stopcock 3, Figure K, Supporting Information) was then closed to seal pure hydrogen in that line. The vacuum line itself was then re-evacuated to $\geq 10^{-4}$ Torr and then sealed by closing the stopcock to the vacuum pump (stopcock 1, Figure K, Supporting Information), leaving the vacuum line under a static vacuum (but not the reaction bulb, which remained closed during this process). The stopcock connecting the hydrogen tank to the vacuum line (stopcock 3, Figure K, Supporting Information) was then opened, allowing pure hydrogen to fill the vacuum line. The hydrogen pressure in the vacuum line was then adjusted to ca. 740 Torr. The stopcock connecting the Baratron to the vacuum line (stopcock 2, Figure K, Supporting Information) was then closed, sealing a known pressure of hydrogen (ca. 740 Torr) in a known volume ($V_{\text{baratron}} + V_{\text{arm}}$). The initial millimoles of hydrogen, $n_{\text{hydrogen(initial)}}$, can then be calculated using the ideal gas law where P = the initial pressure in Torr, V = 26.65 mL ($V_{\text{baratron}} + V_{\text{arm}}$), T = temperature, and R = 62.36 mL Torr K^{-1} $mmol^{-1}$.

Next, the reaction solution, still frozen in the sealed in the reaction bulb, was thawed and brought to room temperature (22.7 °C). The reaction bulb was then submerged in a 500 mL water-jacketed reaction flask (22.0 °C, Figure K, Supporting Information), vortex stirring was initiated, and hydrogen gas was introduced to the solution by opening the reaction bulb (stopcock 4). The total pressure in the assembly, $P_{\text{total}} = p_{\text{Hydrogen}} + p_{\text{solvent}}$, was then monitored over time via the Baratron pressure transducer. (The initial total pressure in this experiment was 273.0 Torr hydrogen ($n_{\text{hydrogern(initial)}} = 1.071$ mmol).

By ca. 4 h, the reaction solution had become light brown; after ca. 4.5 h, it was dark brown/black. After 7.5 h, the reaction was stopped by sealing the reaction flask by closing the stopcock and then transferring the sealed flask into the drybox. The reaction solution was deep blue/black at this point, and a trace of precipitate was visible on the bottom of the reaction flask. Once in the drybox, the flask was opened and the solution was decanted into a screw-cap vial for storage. GLC, Figure N, Supporting Information, confirmed that 1.0 ± 0.1 equiv of cyclooctane evolved from the precursor. A total of 3.9 ± 0.4 equiv of hydrogen per mole of rhodium had been consumed, Figure 5.

In order to test the catalytic activity of this solution, 0.4 mL of this deep blue solution was drawn using a gastight syringe and added to 2.1 mL of propylene carbonate and 0.5 mL of cyclohexene. The resulting dark blue solution was then transferred via polyethylene pipet to a culture tube and placed inside of the Fischer-Porter bottle, and a hydrogenation run was carried out at 22 °C, beginning with 40 psig H_2. The cyclohexene hydrogenation reaction proceeded immediately (i.e., without an induction period) and at an initial rate of 11.7 mmol of H_2/h.

As a control experiment to verify the techniques and methods used herein, we repeated our hydrogen gas-uptake experiment beginning with the iridium complex $[(n\text{-}C_4H_9)_4N]_5Na_3[(1,5\text{-COD})Ir{\cdot}P_2W_{15}Nb_3O_{62}]$, only now in propylene carbonate vs the previously used solvent, acetone.[3] The results (3.6 ± 0.4 equiv, Figure D, Supporting Information) are in agreement with our previously published data in acetone, in which this complex consumes 3.5 ± 0.3 equiv of hydrogen and releases 1.0 ± 0.1 equiv of cyclooctane in the formation of Ir(0) nanoclusters.[3] Additionally, the hydrogen gas-uptake experiments were performed separately with both **1** and $[(1,5\text{-COD})Ir{\cdot}P_2W_{15}Nb_3O_{62}]^{8-}$ in acetone, 1,2-dichloroethane, and acetonitrile; these results are summarized in Table B of the Supporting Information.[27]

Acknowledgment. We wish to thank Dr. Eric Schabtach at the University of Oregon for obtaining the electron diffraction pattern, Professor Anthony K. Rappé for assistance with construction of the metal core models shown in Figure 4, and Kate Weddle for assistance with the ion-exchange chromatography experiments. We also thank Professor Steven H. Strauss for allowing us to use his gas-uptake apparatus. Financial support was provided by the Department of Energy, Chemical Sciences Division, Office of Basic Energy, Grant DOE FG06-089ER13998.

Supporting Information Available: Figure A, energy dispersive spectroscopy of 40 ± 6 Å $Rh(0)_{\sim 2400}$ nanoclusters; Figure B, electron diffraction and Miller indices of the $Rh(0)_{\sim 2400}$ nanoclusters; Figure C, UV−visible spectrum of the $Rh(0)_{\sim 2400}$ nanoclusters in acetonitrile; Table A, elemental analysis data of four samples of polyoxoanion- and tetrabutylammonium-stabilized $Rh(0)_{\sim 2400}$ nanoclusters; Figure D, control experiment showing uptake of 3.6 ± 0.4 equiv of H_2/mol of Ir; Figure E, TEM of effluent from cation-exchange chromatography control experiment done on the Rh(0) nanoclusters; Figure F, hydrogen pressure vs time in a standard conditions hydrogenation reaction beginning from Hg(0) pretreated precatalyst **1**; Figure G, hydrogen pressure vs time in two back-to-back standard conditions hydrogenation reactions beginning from the precatalyst **1** and isolated Rh nanoclusters; Figure H, hydrogen pressure vs time in a standard conditions hydrogenation reaction beginning from the precatalyst **1** and in the presence of 4.0×10^3 equiv of elemental Hg(0); Figure I, detailed schematic of the hydrogenation apparatus used in the present study; Figure J, TEM image (at 300K magnification) of a solution of **1** showing that nanoclusters are not formed from **1** under the TEM conditions; Figure K, detailed schematic of H_2 gas-uptake apparatus used in the present study; Figure L, kinetic curve-fit of cyclooctane equivalents vs time; Figure M, Experimental details and TEM of effluent from cation-exchange chromatography control experiment done on the Ir nanoclusters; Figure N, GLC showing 1.0 ± 0.1 equiv of cyclooctane in the H_2 gas-uptake experiment beginning with **1**; Table B, summary of all H_2 gas-uptake experiments performed as a part of this study (in propylene carbonate, dichloroethane, acetone, and acetonitrile); additional investigation and discussion of the infrequent variability on the observed rates beginning with **1**. This material is available free of charge via the Internet at http://pubs.acs.org.

CM980699W